Electrical conductivity and dielectric behaviour of nanocrystalline $NiFe_2O_4$ spinel

2002 J. Phys.: Condens. Matter 14 3221

(http://iopscience.iop.org/0953-8984/14/12/311)

INSTITUTE OF PHYSICS PUBLISHING JOURNAL OF PHYSICS: CONDENSED MATTER

J. Phys.: Condens. Matter **14** (2002) 3221–3237 PII: S0953-8984(02)32387-7

Electrical conductivity and dielectric behaviour of nanocrystalline $NiFe_2O_4$ spinel

N Ponpandian[1], **P Balaya**[2] **and A Narayanasamy**[1,3]

[1] Materials Science Centre, Department of Nuclear Physics, University of Madras, Guindy Campus, Chennai 600025, India
[2] Max-Planck-Institute for Solid State Research, Heisenbergstraße 1, D 70569 Stuttgart, Germany

E-mail: ansuom@yahoo.co.in (A Narayanasamy)

Received 7 January 2002, in final form 14 February 2002
Published 15 March 2002
Online at stacks.iop.org/JPhysCM/14/3221

Abstract

Electrical conductivity and dielectric measurements have been performed for nanocrystalline $NiFe_2O_4$ spinel for four different average grain sizes, ranging from 8 to 97 nm. The activation energy for the grain and grain boundary conduction and its variation with grain size have been reported in this paper. The conduction mechanism is found to be due to the hopping of both electrons and holes. The high-temperature conductivity shows a change of slope at about 500 K for grain sizes of 8 and 12 nm and this is attributed to the hole hopping in tetrahedral sites of $NiFe_2O_4$. Since the activation energy for the dielectric relaxation is found to be almost equal to that of the dc conductivity, the mechanism of electrical conduction must be the same as that of the dielectric polarization. The real part ε' of the dielectric constant and the dielectric loss $\tan\delta$ for the 8 and 12 nm grain size samples are about two orders of magnitude smaller than those of the bulk $NiFe_2O_4$. The anomalous frequency dependence of ε' has been explained on the basis of hopping of both electrons and holes. The electrical modulus analysis shows the non-Debye nature of the nanocrystalline nickel ferrite.

1. Introduction

In nanocrystalline materials the physical properties are predominantly controlled more by the grain boundaries than by the grains. Spinel ferrites have high electrical resistivities and consequently low eddy currents and dielectric losses. They find wide applications in microwave devices, computer memories and magnetic recording. Spinel ferrites have the general chemical formula $(M^{2+}_{1-\delta}Fe^{3+}_{\delta})[M^{2+}_{\delta}\ Fe^{3+}_{2-\delta}]O^{2-}_{4}$ [1]. The divalent metal ions M^{2+} can occupy either tetrahedral (A) or octahedral (B) sites or both the sites of the spinel ($MgAl_2O_4$) structure

[3] Author to whom any correspondence should be addressed.

depending upon the system. The inversion parameter δ is a measure of the fraction of Fe^{3+} ions at A sites. The strong interaction between magnetic ions in the A and B sites gives rise to ferrimagnetic ordering.

Recently spinel ferrites have been shown to exhibit interesting magnetic properties in the nanocrystalline form compared with those of the micrometre-size grains [2–7]. In our earlier study [7] we reported that $NiFe_2O_4$, in the nanocrystalline form, exhibits a mixed spinel structure with Ni^{2+} ions occupying both A and B sites, but the bulk $NiFe_2O_4$ is a well known inverse spinel, with Ni^{2+} ions occupying only the B sites. Because of this structural change nanocrystalline $NiFe_2O_4$ was shown to exhibit interesting magnetic properties with respect to spin structure, Curie temperature, coercivity etc [6, 7]. Several reports are available in the literature on the electrical conductivity and dielectric properties of bulk $NiFe_2O_4$. However, to our knowledge, such reports are not available, so far, for the nanocrystalline spinel ferrites in general and nanocrystalline $NiFe_2O_4$ in particular. This has motivated us to carry out electrical and dielectric measurements of nanocrystalline $NiFe_2O_4$. In this paper we report the impedance measurements on nanocrystalline $NiFe_2O_4$. The conduction due to grain and grain boundary, the mechanism of conduction and the effect of grain size on conductivity, the dielectric constant and dielectric loss have been studied. The electrical relaxation data have been analysed using modulus spectroscopy to investigate whether the nanocrystalline $NiFe_2O_4$ exhibits Debye- or non-Debye-like relaxation.

2. Experimental details

The bulk $NiFe_2O_4$ spinel was prepared by thoroughly mixing NiO and α-Fe_2O_3 in the atomic ratio 1:1, heating the mixture slowly to 900 °C in air and keeping it at this temperature for 5 h. The powder was then ground in an agate mortar and pelletized with an applied pressure of 50 MPa. The pellets were sintered at 1150 °C for 5 h. The formation of the spinel phase was verified using the x-ray powder diffraction (XRD) technique with the help of a Rigaku-make high-precision Guinier x-ray diffractometer, with Mo Kα radiation of wavelength $\lambda = 0.709\,26$ Å. The milling of the as-prepared ferrite (sample A) was carried out in a high-energy ball mill (Fritsch Pulverisette P7) using zirconia balls and vials at room temperature (RT) with a ball to powder ratio of 8:1 for 40 h to prepare nanocrystalline $NiFe_2O_4$ (sample B). The milled sample was found to retain the spinel phase and no impurity phase was detected. Part of sample B was annealed at 500 °C for 2 h (sample C) and another part was annealed at 1200 °C for 15 h (sample D). The average grain sizes were determined from the (311) reflection of the XRD patterns using the Scherrer formula [8].

The impedance and dc conductivity measurements were performed for all four samples. Nanocrystalline $NiFe_2O_4$ powder was made into pellets of 8 mm diameter and 1 mm thickness for impedance measurements. Prior to the measurements, the sample, which is spring loaded between Pt electrodes, was heated to 150 °C, so as to homogenize the charge carriers and to remove simultaneously the moisture content therein. The real (Z') and imaginary (Z'') parts of the complex impedance (Z^*) were measured as a parametric function of both frequency and temperature in the range 5 Hz–15 MHz and 300–600 K respectively, using an impedance/gain phase analyser (Solartron 1260) together with a dedicated computer and software to acquire the impedance data. Shielded test leads were used for electrical connections from the analyser to the sample to avoid any parasitic impedance due to connecting cables. The heating rate was 2 °C min^{-1}. The temperature of the furnace was measured with a resolution of ± 1 °C using a Eurotherm (818 P) PID temperature controller. The data were collected during both heating and cooling cycles. It was found that the data were consistent during both the thermal cycles. The conductivity (σ) and the real (ε') and imaginary (ε'') parts of the dielectric constant ε^*

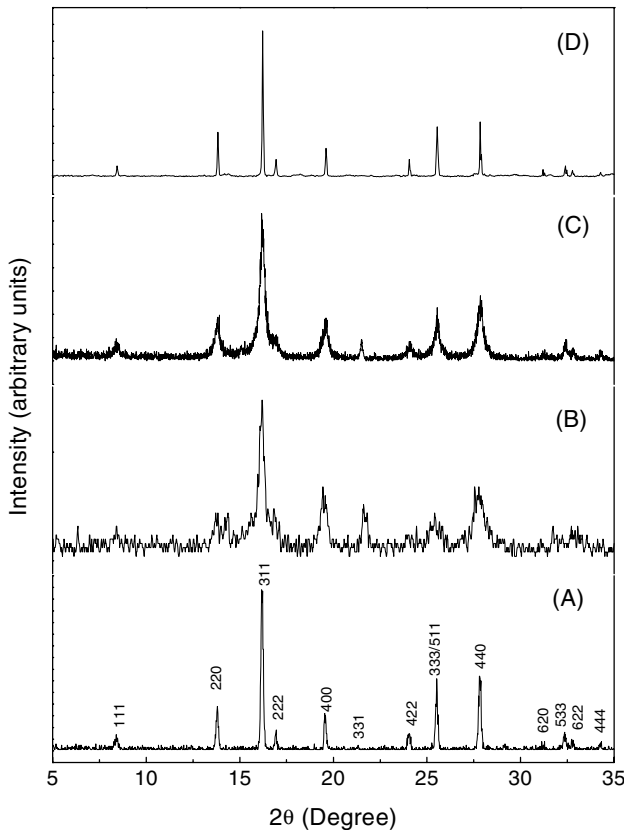

Figure 1. XRD patterns of the $NiFe_2O_4$ spinel samples (A) as prepared, (B) milled for 40 h, (C) milled sample annealed at 500 °C for 2 h and (D) milled sample annealed at 1200 °C for 15 h.

as well as real (M') and imaginary (M'') parts of the complex electric modulus, M^*, were calculated using the raw data of Z' and Z'' and the sample dimensions.

3. Results and discussion

3.1. Crystal structure

Figure 1 gives the XRD patterns of samples A–D. The increase in the width of the x-ray diffraction lines gives evidence for the decrease of the mean particle size of the ball-milled sample. The average particle sizes were found to be 70, 8, 12 and 97 nm for samples A, B, C and D respectively.

3.2. Electrical properties

3.2.1. Dc conductivity. Impedance measurements were carried out for all the samples at selected temperatures in the frequency range 5 Hz–15 MHz. Figure 2 shows the impedance plot for sample A at RT. This consists of two semicircular arcs. The arc on the low-frequency side is due to the grain boundary conduction and that on the high-frequency side is due to the grain conduction; the latter is shown as an inset to figure 2. The equivalent circuit based on the impedance data for the as-prepared sample is shown in figure 3. The parameters R_g, C_g and

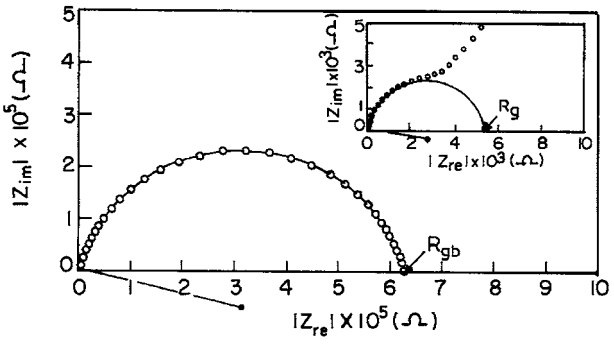

Figure 2. Complex impedance spectrum of sample A. The continuous curves are the fitted semicircles. The inset shows a magnification of the high-frequency region corresponding to the grain conduction.

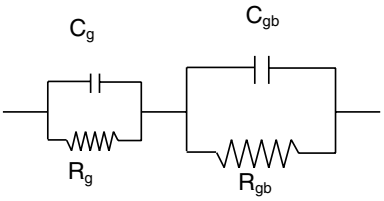

Figure 3. Proposed model for the impedance behaviour shown in figure 2 where C_g is the bulk capacitance, R_g is the bulk resistance, C_{gb} is the grain boundary capacitance and R_{gb} is the grain boundary resistance.

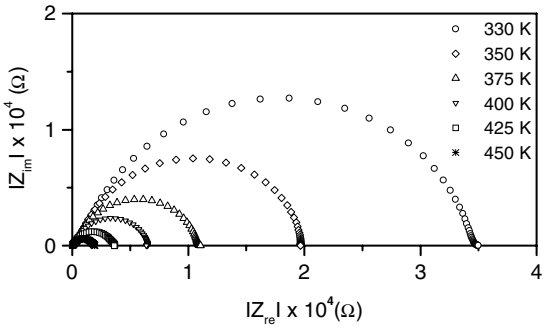

Figure 4. Complex impedance spectra for sample A at various temperatures.

$(\omega_p)_g$ correspond to the resistance, capacitance and the relaxation frequency $(=1/\tau)$ of the grain and R_{gb}, C_{gb} and $(\omega_p)_{gb}$ are the corresponding quantities for the grain boundary. These parameters were obtained for each temperature by analysing the data using the non-linear least-squares (NLLS) fitting routine. The resistance values R_g and R_{gb} were used to calculate the dc conductivity of the grain and the grain boundary respectively. For the as-prepared sample (sample A) and sample D, two semicircles corresponding to the conduction due to grain and grain boundary were obtained whereas only one semicircle was obtained for the other two samples, B and C, suggesting a predominant contribution from the grain boundary and that the contribution from the grain is not well resolved in the present study. Hence we presume that the conductivity for samples B and C is mainly due to the grain boundary contribution. Figure 4 presents

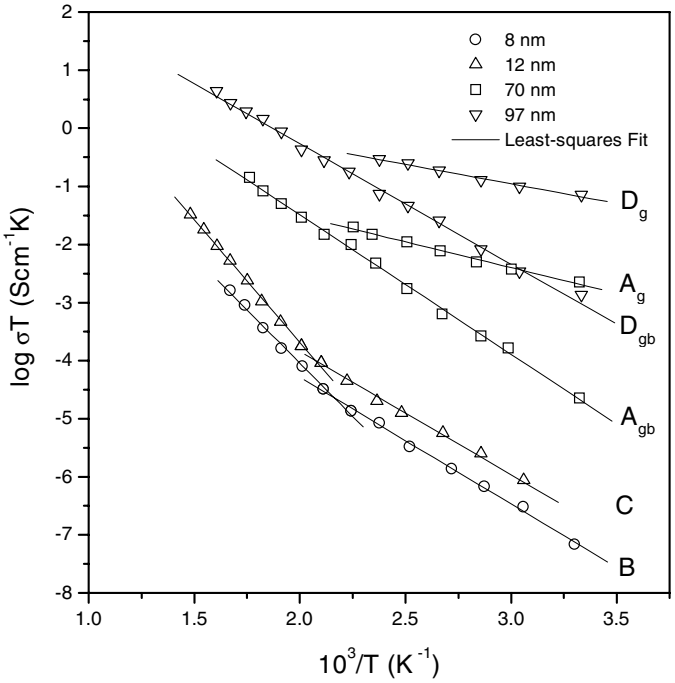

Figure 5. Arrhenius plots of the $NiFe_2O_4$ spinel samples. The solid lines are the best fit to equation (1) (g, grain, and gb, grain boundary).

Table 1. Relaxation frequencies of $NiFe_2O_4$ for four different grain sizes at different temperatures.

Temperature (K)	ω_p(kHz)			
	97 nm	70 nm	12 nm	8 nm
373	630	139	3.3	3.0
423	1725	695	24.0	17.0
473	8976	2261	130.0	83.0

the measured complex impedance spectra for sample A at six different temperatures. Similar measurements have also been made for other samples. The relaxation frequency (ω_p) for the grain boundary shifts to lower values with the decrease in crystallite size as shown in table 1.

Figure 5 shows the temperature dependence of the dc conductivities due to both the grain and grain boundary of samples A and D and that of the grain boundary for samples B and C. The conductivity is found to increase with temperature and grain size. Since the activation energies for the grain boundary conduction are nearly the same up to 500 K, the conductivity mechanism should be the same, for all the samples, in this temperature range. However, for samples B and C there is a change in the slope of the curve beyond approximately 500 K. It is well known that electron hopping between Fe^{2+} and Fe^{3+} ions and hole hopping between Ni^{3+} and Ni^{2+} ions in B sites, with an activation energy $\approx$0.45 eV, are responsible for electrical conduction and dielectric polarization in bulk $NiFe_2O_4$ [9]. The values of activation energies obtained in this study also suggest that the hopping of charge carriers is responsible for the electrical conductivity. In such a hopping process, the carrier mobility is temperature dependent, characterized by an activation energy, which corresponds to the energy picture of

Table 2. The values of activation energies of $NiFe_2O_4$ with various grain sizes. E_a is the activation energy obtained from the conductivity data for the low-temperature region (<500 K) and E'_a is that for the high-temperature region (>500 K). E_p is the activation energy obtained from the hopping frequency for the low-temperature region (<500 K) and E'_p is that for the high-temperature region (>500 K).

Grain size (nm)	Activation energy from conductivity data		Activation energy from hopping frequency	
	E_a (eV)	E'_a (eV)	E_p (eV)	E'_p (eV)
97	0.44	—	0.43	—
70	0.47	—	0.46	—
12	0.48	0.73	0.45	0.72
8	0.50	0.83	0.48	0.82

the crystal lattice around the site of electrons. The increase in dc conductivity with temperature is due to the increase in the thermally activated drift mobility of charge carriers according to the hopping conduction mechanism. The activation energy for the thermally activated hopping process was obtained by fitting the dc conductivity data with the Arrhenius relation,

$$\sigma T = \sigma_0 \exp\left[\frac{-E_a}{kT}\right] \tag{1}$$

where σ_0 is the pre-exponential factor with the dimensions of $(\Omega\ \mathrm{cm})^{-1}$ K, E_a is the activation energy for dc conductivity and k is the Boltzmann constant. The activation energy E_a for the grain conduction in samples A and D was obtained as 0.17 and 0.13 eV. The values of E_a for the grain boundary conduction are given in table 2. As seen from table 2, the value of E_a for the grain boundary conduction increases with grain size reduction. The slight increase in the activation energy and decrease in conductivity reflect the blocking nature of the grain boundary.

Since the activation energies (E'_a) are higher for temperatures above 500 K, the conduction mechanism for this temperature region must be different from that for the temperature region below 500 K. In ferrites the electrons are localized and there is little overlap between the wavefunctions of ions on adjacent sites. As a result, the electrons/holes are not free to move through the lattice. However, in the presence of the lattice vibrations the ions occasionally come close enough that the transfer of electrons from one ion to another occurs with a high probability. Hence the carrier mobility is temperature dependent, characterized by activation energy. In ferrites the distance between the cations in A sites (0.357 nm) is larger than the distance between cations (0.292 nm) in B sites [7] and also the degree of covalency for the A-site ions is known to be higher than that of the B-site cations. Because of this structural difference and the higher degree of covalency in A sites, the mobility of the holes due to $Ni^{2+} \leftrightarrow Ni^{3+}$ transitions in the A sites is expected to be smaller with a higher activation energy than that in the B sites. The conduction due to holes in A sites can therefore be appreciable only at a higher temperature compared with that of the holes in the B sites. The increase in the slope of the σT versus $1/T$ plot beyond 500 K can therefore be attributed to the start of conduction due to the holes in A sites. As the number of Ni ions occupying the A sites has been reported to increase with grain size reduction [7], the slope and hence the activation energy increases with grain size reduction. Samples A and D with grain sizes 70 and 97 nm do not exhibit any change in the slope of the σT versus $1/T$ plot beyond 500 K as the grain sizes for these samples are very high and hence the ferrite will be exhibiting only the inverse spinel structure with all the Ni^{2+} ions occupying the B sites only. For samples B and C, the σT versus $1/T$ plot shows two slopes, the slope of the former being higher than that of the latter, and this is commensurate with the higher number of Ni ions in A sites for sample B.

The decrease in conductivity with grain size reduction may be attributed to the size effects as reported in [10, 11] and also due to the increase in grain boundary volume and the associated impedance to the flow of charge carriers. If the crystallite size is smaller than the electron mean free path, grain boundary scattering dominates and hence the electrical resistivity as well as the temperature coefficient are expected to increase. The electrical resistivity is also very sensitive to lattice imperfections in solids, such as vacancies and dislocations. As pointed out by Bakonyi *et al* [12], besides the crystallite boundaries, the presence of a large number of other types of lattice imperfection has also been found to have an effect on the electrical resistivity in nanocrystalline materials. The change in cation distribution in nanocrystalline $NiFe_2O_4$ may also contribute to the observed decrease in conductivity. Normally the bulk $NiFe_2O_4$ is an inverse spinel with all nickel ions in B sites and the iron ions equally distributed between A and B sites, but in our earlier work [7] it was reported that $NiFe_2O_4$ exhibits a mixed spinel structure when the grain size is reduced to a few nanometres. In the mixed spinel structure some of the nickel ions occupy the A sites, displacing an equal number of iron ions to the B sites. If the hopping frequency of the holes through $Ni^{3+} \leftrightarrow Ni^{2+}$ pairs in A sites is smaller than that in B sites, the conductivity should decrease with grain size reduction as the number of nickel ions occupying the A sites has been reported to increase with decrease in grain size [7].

The conductivities of samples B, C and D were also measured at a fixed frequency (110 Hz) as a function of temperature with a close scanning of temperature. It is observed that the grain boundary conductivity of sample D with a grain size of 97 nm is due to a simple hopping mechanism with a single activation energy, while samples B (8 nm) and C (12 nm) clearly exhibit two semiconducting regions with two different activation energies as seen from figure 6. This behaviour is found to be in agreement with that observed from the complex impedance measurements as discussed earlier. However, the activation energies were found to be about 15% higher than those obtained from the complex impedance measurements. Since the resistance obtained from the complex impedance measurements should be more accurate than the resistance from measurements at a fixed frequency, we prefer to consider the values of the activation energies obtained from the complex impedance measurements for further discussions.

Figure 7 shows the plot of hopping frequency versus temperature. This hopping frequency refers to the dipolar orientational relaxation frequency. The temperature dependence of the dielectric relaxation frequency ω_p could be written in the following form [13]:

$$\omega_p = \omega_0 \exp\left[\frac{-E_p}{kT}\right] \tag{2}$$

where ω_0 is the pre-exponential factor, E_p is the activation energy for dielectric relaxation and k is the Boltzmann constant. It is interesting to note that the hopping frequencies for all the samples have a temperature dependence similar to that of the dc conductivity. The increase in relaxation frequency with temperature is due to the thermal activation of the localized electric charge carriers forming dipoles, which are responsible for dielectric polarization [14]. The activation energy E_p for dielectric relaxation was calculated from the slope of the straight lines in figure 7 for various grain sizes. In table 2, a comparison is made between E_p for the dielectric relaxation and the values of E_a for the dc conduction. Since they are almost equal, it is noted that the mechanism of electrical conduction is the same as that of dielectric polarization in these ferrites [15].

It is known that the main features of dielectric loss in conducting materials are (i) very broad dielectric loss peaks with a temperature-independent shape and an almost frequency-independent loss at high frequencies and (ii) an Arrhenius temperature-dependent dielectric loss peak frequency ω_p with the same activation energy as that of the dc conductivity. This means that the ω_p and σ_{dc} are proportional and the constant of proportionality is almost

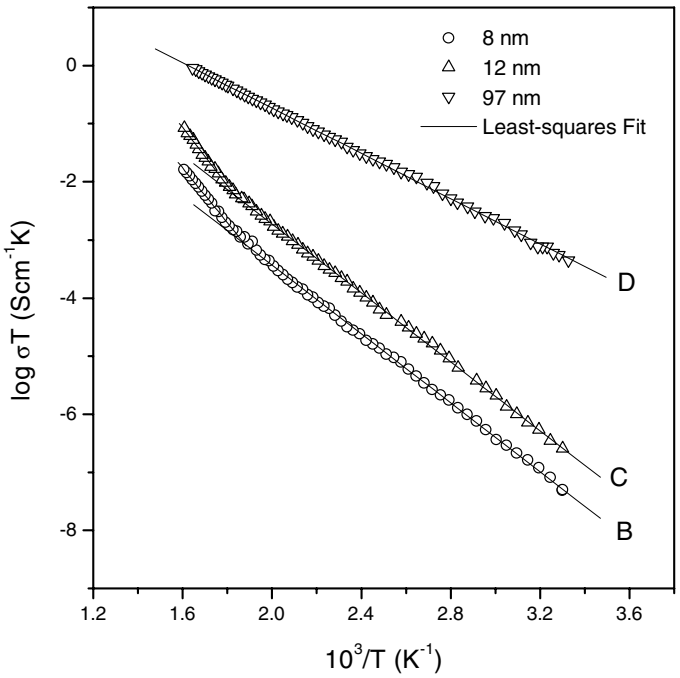

Figure 6. The temperature dependence of the dc conductivity at 110 Hz for samples B, C and D. The solid lines are the best fit to equation (1).

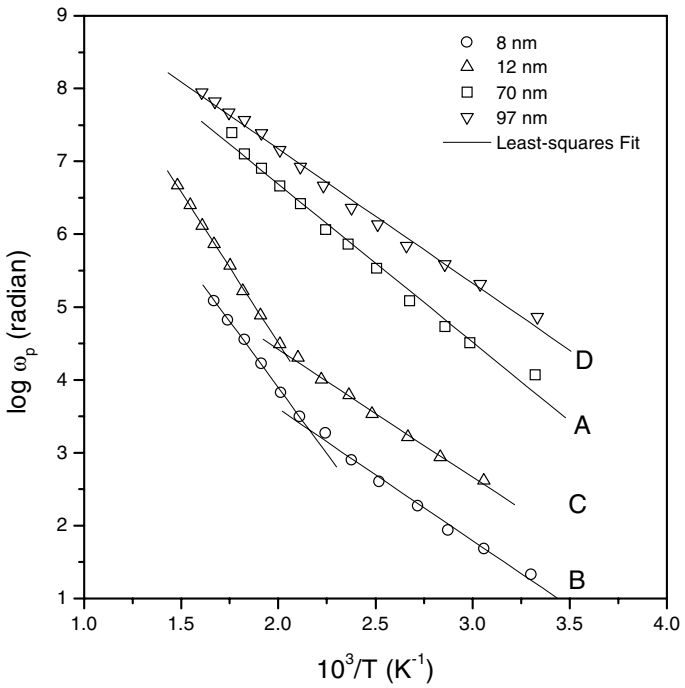

Figure 7. The temperature dependence of the dielectric relaxation frequency ω_p of the four samples. The solid lines are the best fit to equation (2).

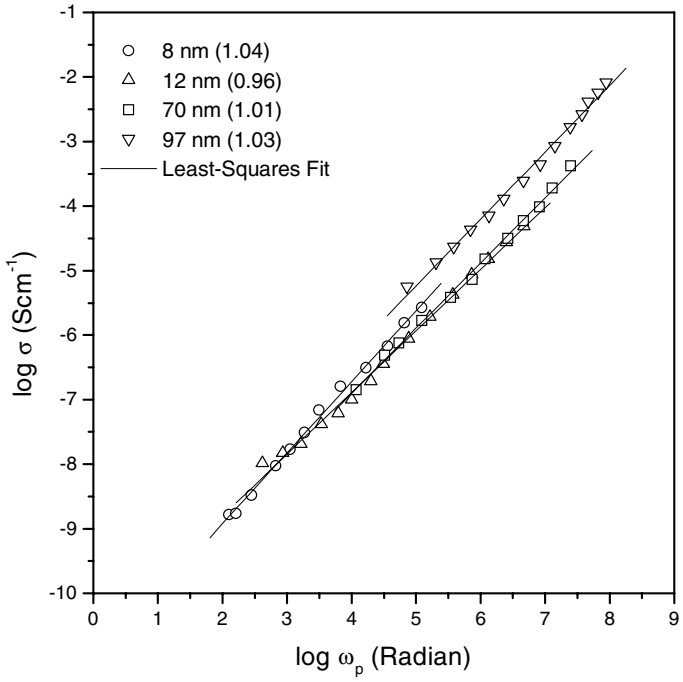

Figure 8. $\log_{10}\sigma_{dc}$ versus $\log_{10}\omega_p$ plots for the four samples illustrating that $\sigma_{dc} \propto \omega_p$. The solid lines are the least-squares fits. The values of the slopes are given in the parentheses.

universal, varying only weakly with temperature. A closer analysis of the proportionality was carried out by Barton, Nakajima and Namikawa (BNN), who found the following equation to be valid for most of the conductive materials:

$$\sigma_{dc} = \frac{1}{4\pi H_R}\varepsilon_0 \Delta\varepsilon \omega_p \tag{3}$$

where H_R is the Haven ratio, which indicates the degree of correlation between the successive hops, ε_0 is the free-space permittivity, $\Delta\varepsilon$ $(=\varepsilon(0) - \varepsilon(\infty))$ is the permittivity change from the unrelaxed baseline $(\varepsilon(\infty))$ to the fully relaxed level $(\varepsilon(0))$ and ω_p is the hopping frequency. The BNN relation conveys the important information that ac and dc conductions are closely correlated to each other and that they are of the same mechanism. Our interest is to find whether the BNN relation is obeyed in the case of nanocrystalline $NiFe_2O_4$ or not. For this purpose we have plotted $\log_{10}\sigma_{dc}$ versus $\log_{10}\omega_p$ in figure 8 for various crystallite sizes, where the values of σ_{dc} and ω_p were obtained from the best fits from the NLLS fitting. The solid lines are the least-squares straight-line fits, all of which give a slope almost equal to unity, implying that the dc and ac conductions are correlated with each other in nanocrystalline $NiFe_2O_4$ and that they are governed by the same mechanism [16].

3.2.2. Conduction mechanism. The temperature dependence of dc conductivities of the samples with grain sizes 8 and 12 nm exhibits two semiconducting regions, one with an average E_a of 0.47 eV for the low-temperature region and the other with an average E_a of 0.78 eV for the high-temperature region. In order to understand the conduction mechanism in the milled ferrite (sample B) we measured the capacitance of the sample for various bias voltages (potential) as reported by Na *et al* [17]. Figure 9 shows the plot of $1/C^2$ versus bias

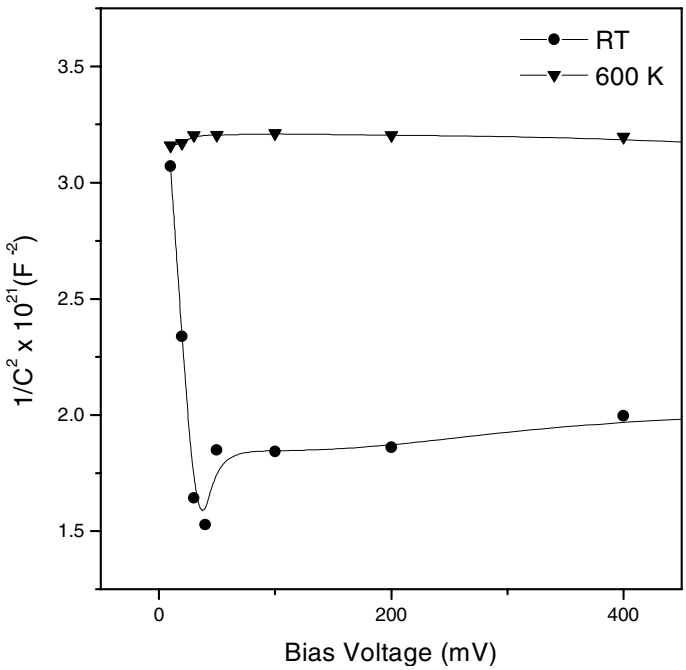

Figure 9. $1/C^2$ versus bias voltage plot for the $NiFe_2O_4$ spinel with 8 nm average grain size (sample B) at RT and 600 K. The continuous curve is a guide to the eye.

voltage for the sample with 8 nm grain size at RT and at 600 K. At RT the capacitance decreases initially, reaches a minimum, increases slightly and almost saturates at high bias voltages. The negative slope for small bias voltages suggests that the initial conduction is due to electrons. At higher bias voltages, holes also take part in conduction, resulting in a flat curve. However, $1/C^2$ versus bias voltage at 600 K gives a flat response, suggesting that both the electrons and the holes play competing roles for the conduction at this temperature. This response is similar to that at RT for high bias voltages. Either high bias or high temperature enables both holes and electrons to take part in the conduction process. This measurement makes it clear that the low-temperature conductivity is mainly due to electrons and at high temperatures both electrons and holes take part in conduction.

3.2.3. Dielectric behaviour. The existence of Fe^{3+} ions and the minority Fe^{2+} ions have rendered ferrite materials dipolar. Rotational displacements of the dipoles result in orientational polarization. In the case of ferrites, the rotation of Fe^{2+}–Fe^{3+} dipoles may be visualized as the exchange of electrons between the ions so that the dipoles align themselves with the alternating field. The existence of inertia to the charge movement would cause a relaxation to the polarization. The effects of frequency (ω) on the dielectric constant ε' and dielectric loss factor $\tan\delta$ (at 373 K) for samples with various crystallite sizes are illustrated in figures 10 and 11 respectively. In the literature the real part ε' of the dielectric constant has been reported to be of the order of 10^4 at 373 K for the bulk $NiFe_2O_4$ [9]. In our measurements ε' is found to be two orders of magnitude smaller for the nanocrystalline $NiFe_2O_4$ of grain sizes 8 and 12 nm. Similarly the dielectric loss is also found to be two orders of magnitude smaller for the grain sizes of 8 and 12 nm.

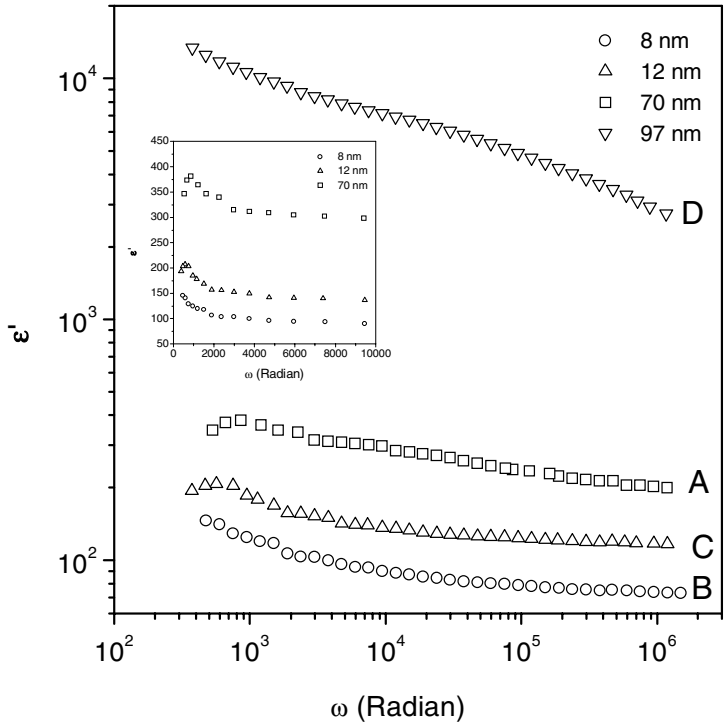

Figure 10. The real part ε' of the dielectric constant at 373 K as a function of frequency for four samples of $NiFe_2O_4$.

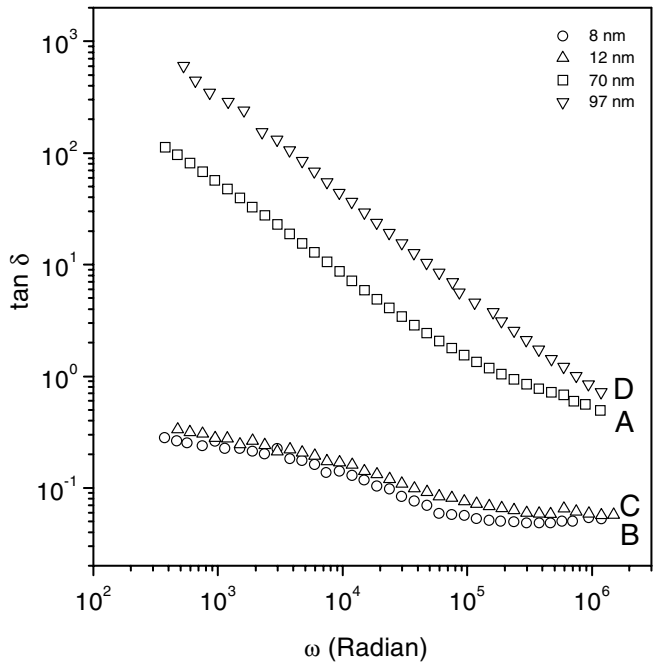

Figure 11. The dielectric loss factor tan δ at 373 K as a function of frequency for four samples of $NiFe_2O_4$ spinel.

The dielectric constant ε' shows an anomalous behaviour with frequency for samples A, B and C. It initially increases with frequency, reaches a maximum and then decreases with further increase in frequency. The value of ε' decreases and the peak position shifts to a lower frequency on grain size reduction. In the normal behaviour, the polarization (or dielectric constant) will monotonically decrease with frequency as in the case of sample D. This happens as the electronic exchange between $Fe^{2+} \leftrightarrow Fe^{3+}$ cannot follow the alternating field beyond a certain frequency. In $NiFe_2O_4$ the presence of Ni^{3+} and Ni^{2+} ions gives rise to p-type carriers. The local displacements of p carriers in the direction of the external electric field also contribute to the net polarization in addition to the n-type carriers. However, the contribution of the p-type carriers should be smaller than that from the electronic exchange between $Fe^{2+} \leftrightarrow Fe^{3+}$ and also it has an opposite sign. Since the mobility of the p-type carriers is smaller than that of the n-type carriers, the contribution to polarization from the former will decrease more rapidly and even at lower frequencies than from the latter. As a result the net contribution will increase initially and then decrease with frequency as observed in the present samples. A similar behaviour has been reported for Cu–Ni ferrites by Rezlescu and Rezlescu [18].

The shift in the position of the maximum towards lower frequencies when the grain size is reduced can be explained by proposing a decrease in the number of p-type carriers in the B sites as has been reported earlier in the case of $Cu_xNi_{1-x}Fe_2O_4$ [18]. Our earlier Mössbauer studies [7] have shown that the number of Ni ions displaced from the B sites to the A sites increases when the grain size is reduced. This will lead to a decrease in the number of $Ni^{3+} \leftrightarrow Ni^{2+}$ pairs and hence the number of available p-type carriers in the B sites. The same mechanism also explains the decrease in the value of ε' with grain size reduction. The real part of the dielectric constant decreases with frequency and also the loss is lower for smaller grain size as the resistivity increases with grain size reduction.

The anomalous temperature dependence of ε' for samples A, B and C, as seen from figure 12, could be explained as in the case of its frequency dependence. The contributions of the two types of carrier to polarization depend on temperature. Since the temperature could influence the electronic exchange $Fe^{2+} \leftrightarrow Fe^{3+}$ more than it could the displacements of p-type carriers, ε' will increase with temperature at the beginning, but above a certain temperature the contribution from the p-type carriers also becomes significant and thus ε' will begin to decrease since the two contributions oppose each other. The dielectric losses, as seen from figure 13, increase as a result of the decreasing resistivity of the samples with temperature. Also, the loss decreases with grain size reduction. The shift of the maximum of the ε' curve for sample B to higher temperatures as noticed from figure 14 with increasing frequency is because of the increase of the hopping frequency of the carriers with temperature. As seen from figure 15, the dielectric loss of sample B increases with temperature as in the case of any dielectric material.

3.2.4. Electrical modulus studies. The electrical relaxation in ionically and electronically conducting materials has been extensively studied and analysed in terms of modulus formalism [19, 20]. The advantage of representing the electrical relaxation in modulus formalism is that the electrode polarization effects are suppressed in this representation. The transition from the frequency-independent to frequency-dependent conductivity indicates the onset of a relaxation phenomenon, which is here analysed in the framework of the modulus formalism. According to Macedo *et al* [20] and Moynihan *et al* [21] the electric modulus was defined as the electric analogue of the dynamical mechanical modulus and was related to the complex permittivity $\varepsilon^*(\omega)$ by

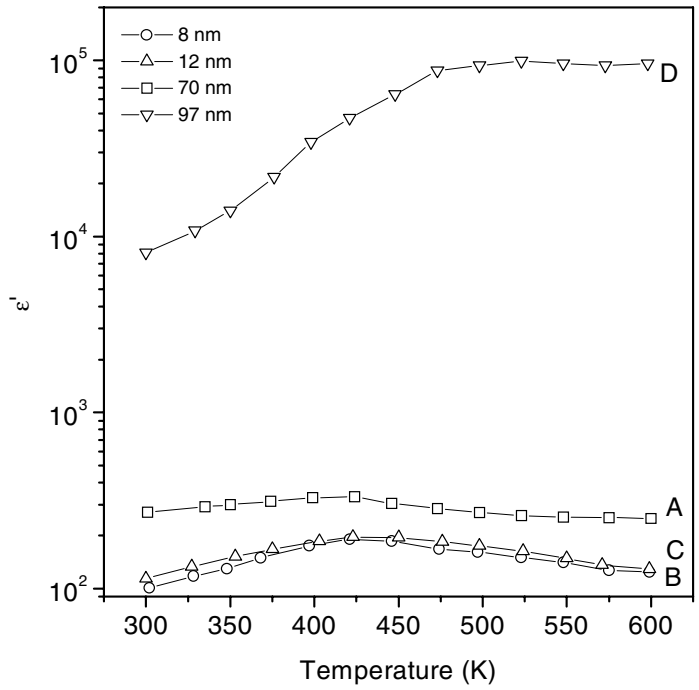

Figure 12. The temperature dependence of ε' for four samples of $NiFe_2O_4$ at 100 Hz.

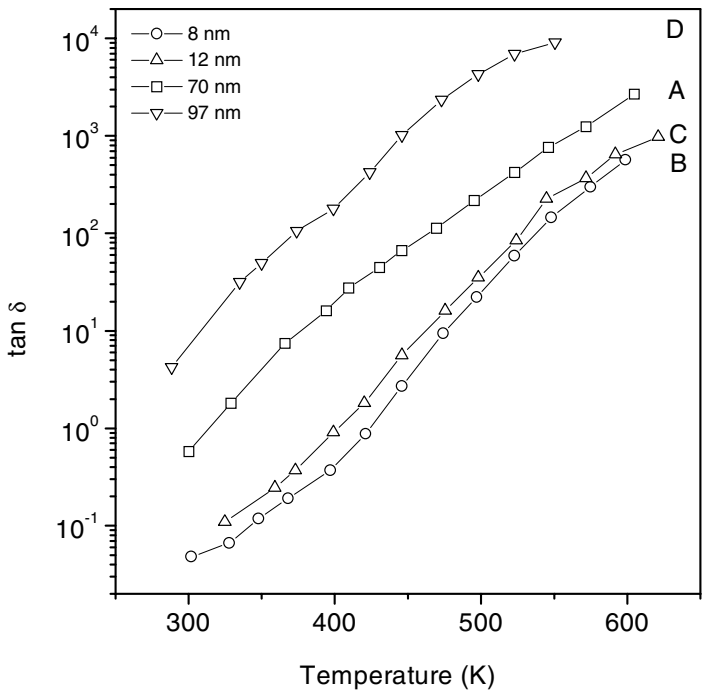

Figure 13. The temperature dependence of tan δ for four samples of $NiFe_2O_4$ at 100 Hz.

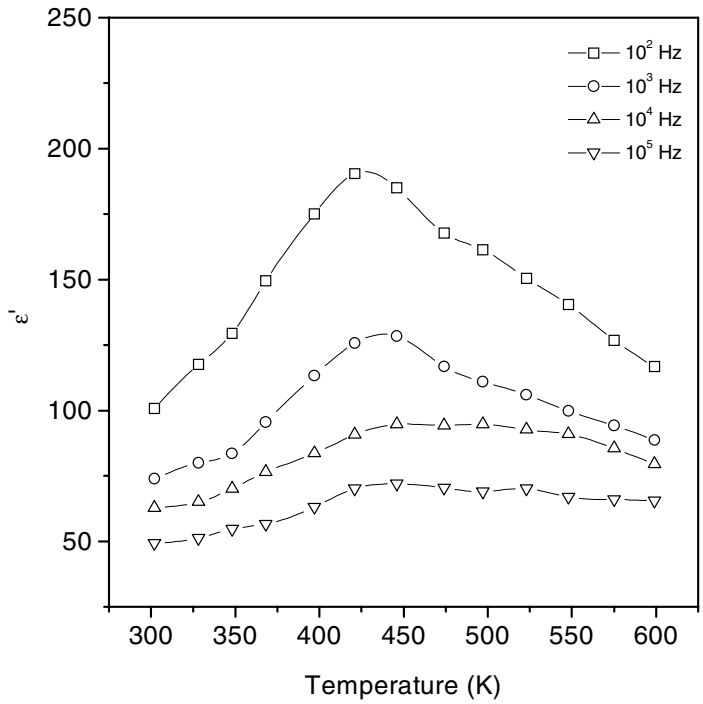

Figure 14. The temperature dependence of ε' at various frequencies for sample B of $NiFe_2O_4$.

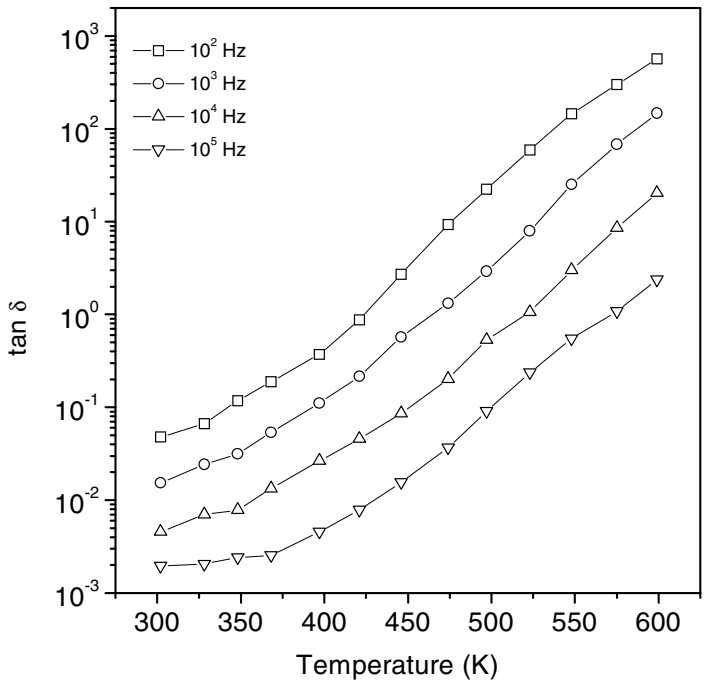

Figure 15. The temperature dependence of tan δ at various frequencies for sample B of $NiFe_2O_4$.

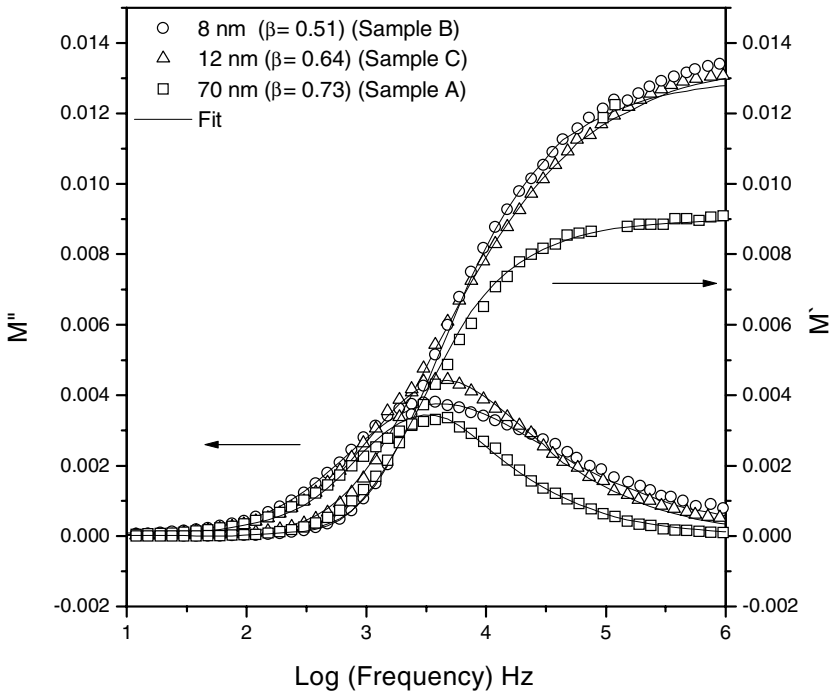

Figure 16. The modulus spectra for samples A, B and C of $NiFe_2O_4$ spinel at 300 K. The solid curves are the best fits to equation (4).

$$M^*(\omega) = \frac{1}{\varepsilon^*(\omega)} = \{\varepsilon'(\omega) - \mathrm{i}\varepsilon''(\omega)\}|\varepsilon^*(\omega)|^2 = M'(\omega) + \mathrm{i}M''(\omega) \tag{4}$$

$$M_\infty \quad = \left[1 - \int_0^\infty \mathrm{e}^{-\mathrm{i}\omega t}\left\{\frac{\mathrm{d}\phi}{\mathrm{d}t}\right\}\mathrm{d}t\right] \tag{5}$$

where $M'(\omega)$ and $M''(\omega)$ are the real and imaginary parts of the electric modulus, $M_\infty = 1/\varepsilon_\infty$ is the inverse of the high-frequency dielectric permittivity and the function $\phi(t)$ gives the time evolution of the electric field within the dielectrics and is related to relaxation time by the decay function proposed by Kohlrausch, Williams and Watts (KWW) [22]; it is given by

$$\phi(t) = \exp\left[-\left(\frac{t}{\tau_m}\right)^\beta\right], \qquad 0 < \beta < 1 \tag{6}$$

where τ_m is defined as the most probable relaxation time and β is the stretched exponent parameter, the value of which decides whether the relaxation in a given material is Debye or non-Debye in nature and is related to the full width at half maximum of a suitably normalized $M''(\omega)$ versus ω curve.

Figure 16 shows the real (M') and imaginary (M'') parts of the electrical modulus for the nanocrystalline $NiFe_2O_4$ for various crystallite sizes at 300 K. The value of β is equal to unity for an ideal dielectric for which the dipole–dipole interaction is negligible, but for the system where dipole–dipole interaction is significant the β value is always less than unity. We fitted the modulus data with the KWW function by varying the β and τ parameters. The β value turned out to be very much less than unity for our $NiFe_2O_4$ samples and the values are given in figure 16. Since the grain boundary volume increases due to the reduction of grain size, the number of dipoles in the grain boundary also increases significantly. As a result

the interaction among the dipoles within the grain boundary increases and hence the dipole relaxation becomes slower, reducing the relaxation frequency. The fact that the value of β is very much less than unity shows the non-Debye nature of nanocrystalline $NiFe_2O_4$. The β-value decreases with grain size reduction, showing that the interaction between the dipoles increases in the grain boundary.

4. Conclusion

The electrical conductivity and dielectric behaviour of nanocrystalline $NiFe_2O_4$ have been studied. The impedance spectra show two semicircles corresponding to grain and grain boundary conductions for the 70 and 97 nm samples and only one semicircle corresponding to the predominant grain boundary contribution for the 8 and 12 nm samples. The values of activation energy obtained are characteristic of the hopping of charge carriers. The activation energy slightly increases with the grain size reduction due to the blocking nature of the grain boundary and lattice imperfections. The change of slope of the Arrhenius plot above 500 K for the 8 and 12 nm samples has been attributed to the conduction due to holes in tetrahedral sites. The dc and ac conductivities are governed by the same mechanism, as the BNN relation is found to be valid, and also due to the fact that the activation energy is the same for both ac and dc conduction. The real part ε' of the dielectric constant and the dielectric loss for the 8 and 12 nm grain size samples are smaller than those of the bulk $NiFe_2O_4$ by two orders of magnitude. The anomalous frequency dependence of ε' has been explained on the basis of hopping of both electrons and holes. The nanocrystalline $NiFe_2O_4$ exhibits non-Debye behaviour with the value of the stretched exponent (β) decreasing with grain size reduction because of the increasing disorder in the grain boundary.

Acknowledgments

The authors would like to thank Professor V R K Murthy for fruitful discussions and for critically going through the manuscript and Dr K Govindarajan for the XRD measurements. The partial financial support from the UGC-SAP (phase III) and the UGC Major Research Project (F.10-32/98 (SR-I)) is gratefully acknowledged. One of us (NP) would like to thank the Council of Scientific and Industrial Research, Government of India, for the award of a senior research fellowship.

References

[1] Smit J and Wijn H P J 1959 *Ferrites* (Eindhoven: Philips)
[2] Chinnasamy C N, Narayanasamy A, Ponpandian N, Chattopadhyay K, Gueralt H and Greneche J-M 2000 *J. Phys.: Condens. Matter* **12** 7795
[3] Oliver S A, Hamdeh H H and Ho J C 1999 *Phys. Rev.* B **60** 3745
[4] Šepelák V, Baabe D and Becker K D 2000 *J. Mater. Synth. Process.* **8** 333
[5] Šepelák V, Baabe D, Litterst F J and Becker K D 2000 *J. Appl. Phys.* **88** 5884
[6] Kodama H and Berkovitz A E 1999 *Phys. Rev.* B **59** 6321
[7] Chinnasamy C N, Narayanasamy A, Ponpandian N, Chattopadhyay K, Shinoda K, Jeyadevan B, Tohji K, Nakatsuka K, Furubyashi T and Nakatani I 2001 *Phys. Rev.* B **63** 184108
[8] Cullity B D 1978 *Elements of X-Ray Diffraction* (London: Addison-Wesley)
[9] Abdeen A M 1999 *J. Magn. Magn. Mater.* **192** 121
[10] Wang Y Z, Qiao G W, Liu X D, Ding B Z and Hu Z Q 1993 *Mater. Lett.* **17** 152
[11] Liu X D, Ding B Z, Hu Z Q, Lu K and Wang Y Z 1993 *Physica* B **192** 345
[12] Bakonyi I, Toth-Kadar E, Tarnoczi T, Varga L, Cziraki A, Gerocs I and Fogarassy B 1993 *Nanostruct. Mater.* **3** 155

[13] Mansingh A, Dhawain V K and Sayer H 1983 *Phil. Mag.* B **48** 21
[14] Van Uitert L G 1955 *J. Chem. Phys.* **23** 1883
[15] Murthy V R K and Sobanadri J 1976 *Phys. Status Solidi* a **36** K133
[16] Dyre J C 1988 *J. Appl. Phys.* **64** 2456
[17] Na J G, Kim M C, Lee T D and Park S J 1993 *IEEE Trans. Magn.* **29** 3520
[18] Rezlescu N and Rezlescu E 1974 *Phys. Status Solidi* a **59** 575
[19] Baskaran N, Govindaraj G and Narayanasamy A 1997 *Solid State Ion.* **98** 217
[20] Macedo P B, Moynihan C T and Bosech R 1972 *Phys. Chem. Glasses* **13** 171
[21] Moynihan C T, Bosech L P and Laberge N L 1973 *Phys. Chem. Glasses* **14** 122
[22] Williams G and Watts D C 1970 *Trans. Faraday Soc.* **66** 80